

Adaptive Cross-Layer Attention for Image Restoration

Yancheng Wang, Ning Xu, Chong Chen, and Yingzhen Yang

Abstract—Non-local attention module has been proven to be crucial for image restoration. Conventional non-local attention processes features of each layer separately, so it risks missing correlation between features among different layers. To address this problem, we propose Cross-Layer Attention (CLA) module in this paper. Instead of finding correlated key pixels within the same layer, each query pixel can attend to key pixels at previous layers of the network. In order to further enhance the learning capability and reduce the inference cost of CLA, we further propose Adaptive CLA, or ACLA, as an improved CLA. Two adaptive designs are proposed for ACLA: 1) adaptively selecting the keys for non-local attention at each layer; 2) automatically searching for the insertion locations for ACLA modules. By these two adaptive designs, ACLA dynamically selects the number of keys to be aggregated for non-local attention at layer. In addition, ACLA searches for the optimal insert positions of ACLA modules by a neural architecture search method to render a compact neural network with compelling performance. Extensive experiments on image restoration tasks, including single image super-resolution, image denoising, image demosaicing, and image compression artifacts reduction, validate the effectiveness and efficiency of ACLA.

Index Terms—Image restoration, non-local attention, cross-layer attention, key selection.

1 INTRODUCTION

IMAGE restoration algorithms aim to recover a high-quality image from a contaminated input image by solving an ill-posed image restoration problem. There are various image restoration tasks depending on the type of corruptions, such as image denoising [1], [2], demosaicing [1], [3], single image super-resolution [4], [5], [6], and image compression artifacts reduction [7]. To restore corrupted information from the contaminated image, a variety of image priors [8], [9], [10] were proposed.

Recently, image restoration methods based on deep neural networks have achieved great success. Inspired by the widely used non-local prior, most recent approaches based on neural networks [1], [2] adapt non-local attention into their neural network to enhance the representation learning, following the non-local neural networks [11]. In a non-local block, a response is calculated as a weighted sum over all pixel-wise features on the feature map to account for long-range information. Such a module was initially designed for high-level recognition tasks such as image classification, and it has been proven to be beneficial for low-level vision tasks [1], [2].

Though attention modules have been shown to be effective in boosting the performance. Most attention modules only explore the correlation among features at the same layer. Actually, features at different intermediate layers encode variant information at different scales, and might be helpful to augment the information used in recovering the high-quality image. Motivated by the potential benefit of exploring feature correlation across intermediate layers,

Holistic Attention Network (HAN) [12] is proposed to find interrelationship among features at hierarchical levels with a Layer Attention Module (LAM). However, LAM assigns a single importance weight to all features at the same layer and neglects the difference of spatial positions of these features. Recent research in omnidirectional representation [13] suggests that exploring the relationship among features at different layers can benefit the representation learning of neural networks. Nevertheless, calculating correlation among features at hierarchical layers is computationally expensive due to the quadratic complexity of dot product attention. The complexity of such cross-layer attention design is increased from $(HW)^2L$ to $(HWL)^2$, where H, W are the height and width of the feature map and L is the number of layers.

1.1 Contributions

Our contributions are listed as follows.

First, in order to address the problem caused by only referring to keys within the same layer in most attention modules, we propose a novel attention module termed Cross-Layer Attention (CLA), which searches for keys across different layers for each query feature. With the help of the deformation mechanism, CLA only attends to a small set of keys at different layers for each query feature.

Second, we propose an improved CLA termed Adaptive Cross-Layer Attention (ACLA) which selects an adaptive number of keys at each layer for each query, and searches for the optimal insert positions of ACLA modules. We deploy ACLA modules on commonly used neural network models, e.g. EDSR [14], for image restoration. Extensive experiments on single image super-resolution, image denoising, image compression artifacts reduction, and image demosaicing demonstrate the effectiveness of our approach.

• *Yancheng Wang and Yingzhen Yang are with School of Computing and Augmented Intelligence, Arizona State University, Tempe, AZ, 85281. E-mail: ywan1053@asu.edu, yingzhen.yang@asu.edu*

• *Chong Chen and Ning Xu are with Kuaishou Technology. E-mail: chongchen@kuaishou.com, ningxu@kuaishou.com*

2 RELATED WORKS

2.1 Neural Networks for Image Restoration

Adopting neural networks for image restoration has achieved great success by utilizing their power in representation. ARCNN [15] was first proposed to use CNN for compression artifacts reduction. Later, DnCNN [7] uses residual learning and batch normalization to boost performance of CNN for image denoising. In IRCNN [3], a learned set of CNNs are used as denoising prior for other image restoration tasks. For single image super-resolution [4], [5], [16], [17], even more efforts have been devoted to designing advanced architectures and learning methods. For example, RDN [16] and CARN [18] fuse low-level and high-level features with dense connection to provide richer information and details for reconstructing. Recently, non-local attention [2], [19], [20] is also used to further boost the performance of CNN for image restoration.

2.2 Attention Mechanism

Attention mechanism has been applied to many computer vision tasks, such as image captioning [21], [22] and image classification [23], [24]. Non-local attention [11] was first proposed to capture long-range dependencies for high-level recognition tasks. Recently, several works propose to leverage non-local attention for low-level vision tasks. In NLRN [2] a recurrent neural network is proposed to incorporate non-local attention. RNAN [1] proposed a residual local and non-local mask branch to obtain non-local mixed attention. RCAN [25] exploits the interdependencies among feature channels by generating different attention for each channel-wise feature. HAN [12] is proposed to find interrelationship among features at hierarchical levels with a layer attention module. Besides, some recent works attempt to explore the benefits of transformer based models for image restoration. IPT [26] is proposed to solve various restoration problems in a multi-task learning framework based on visual Transformer. SwinIR [27] adopt the architecture of Swin Transformer. However, compared with methods using CNN architecture, transformer-based image restoration methods usually use large datasets for training. Specifically, IPT uses ImageNet to pretrain the model. SwinIR adapts a combination of four datasets consisting of over 8000 high-quality images as training set for the tasks of denoising and compression artifact reduction.

2.3 Neural Architecture Search

Neural Architecture Search (NAS) has attracted lots of attention recently. Early works of NAS adopt heuristic methods such as reinforcement learning [28] and evolutionary algorithm [29]. The search process with such methods requires huge computational resources. Recently, various strategies are designed to reduce the expensive costs including weight sharing [30], progressive search [31] and one-shot search [32], [33]. For example, DARTS [32] firstly relaxes the search space to be continuous and conducts differentiable search. The architecture parameters and network weights are trained simultaneously by gradient descent to reduce the search time.

Despite the success of NAS methods for classification, dense prediction tasks such as semantic image segmentation and image restoration, usually demand more complicate network architectures. Some recent works have been devoted to explore hierarchical search space for dense prediction tasks. For example, Auto-DeepLab [34] introduces a hierarchical search space for semantic image segmentation. DCNAS [35] build a densely connected search space to extract multi-level information. HNAS [36] also adopts a hierarchical search space for single image super-resolution.

3 METHOD

3.1 CLA: Cross-Layer Attention

Non-Local Attention. Non-Local (NL) attention [11] is designed to integrate self-attention mechanism into convolutional neural networks for computer vision tasks. It is usually applied on an input feature map $x \in \mathbb{R}^{H \times W \times C}$ to explore self similarities among all spatial positions. We reshape x to $N \times C$, $N = H \times W$, where H, W, C are height, width and channel number of the input feature map X . A generic NL attention can be formulated as

$$y_i = \frac{1}{C(x)} \sum_{n=1}^N f(x_i, x_n)g(x_n), \quad (1)$$

where i indexes the spatial position of feature maps. y is the output of NL attention with the same size as x . $f(x_i, x_n)$ is the pairwise affinity between the query feature x_i and its key feature x_n . $g(x_n)$ computes an embedding of feature x_n . $C(x)$ is a normalization term.

NL attention is usually wrapped into a non-local block [11] with a residual connection from the input feature x . The mathematical formulation is given as

$$z = h(y) + x, \quad (2)$$

where h denotes a learnable feature transformation, which takes the output of non-local attention (1) as input.

Cross-Layer Attention. To search for keys from different layers for each query feature, we propose Cross-Layer Attention (CLA). To derive the formulation of CLA, we start by adapting NL attention in Equation (1) to a cross-layer design, such that features from different layers are regarded as keys. In the sequel, the superscript indicates the index of a layer, and subscript indicates spatial location. Suppose that x^i is the output of the i -th layer in a CNN backbone for image restoration, where $i \in \{1, \dots, L\}$ and L is the number of layers. A vanilla Cross-Layer Non-Local (CLNL) attention is formulated as

$$y_i^j = \frac{1}{C(x^j)} \sum_{l=1}^j \sum_{n=1}^N f(x_i^j, x_n^l)g(x_n^l), \quad (3)$$

where the superscripts j, l index the layer and the subscripts i, n index the spatial locations of features. y, x denote the output feature and input feature respectively. With such adaption, relationships among features across different layers can be captured. However, given the quadratic complexity of correlation computation, the complexity of CLNL is increased from N^2L to $(NL)^2$. In order to mitigate the expensive inference cost, we leverage deformable mechanism

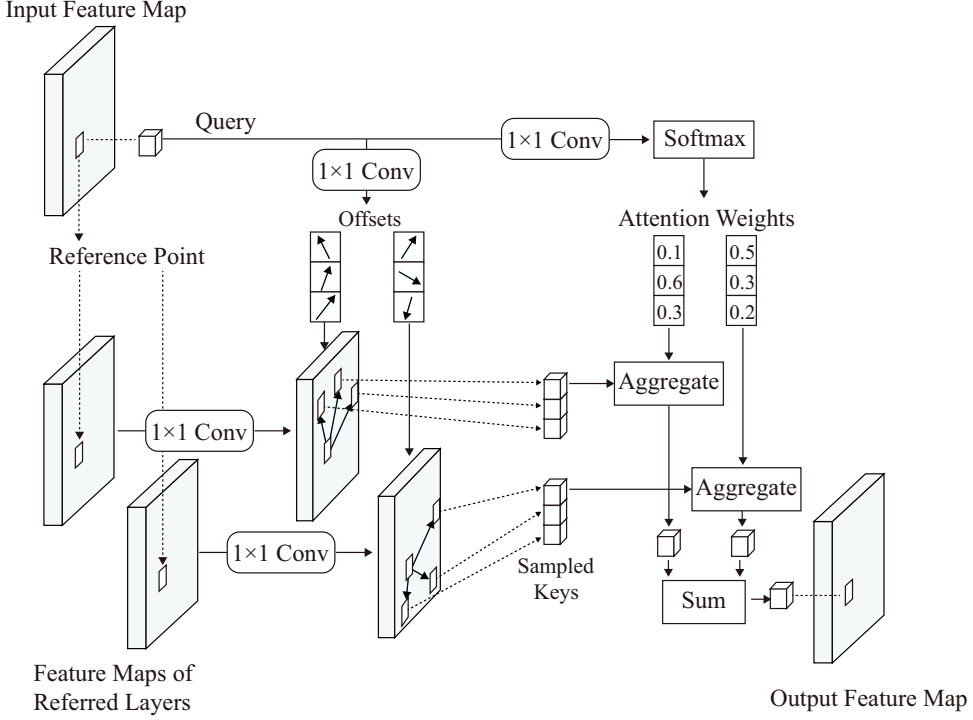


Fig. 1: Illustration of Cross-Layer Attention (CLA) module. For each query pixel, a 1×1 convolution layer is used to obtain the offsets of the positions of keys sampled from the referred layers. Then, a convolution layer and Softmax are applied to the query feature to generate attention weights for sampled keys. Weighted by the attention weights, the features of the sampled keys are aggregated to generate the output of the CLA module.

proposed in deformable convolution (DCN) [37] to design our proposed CLA as

$$y_i^j = \frac{1}{\mathcal{C}(x^j)} \sum_{l=1}^j \sum_{k=1}^K f(x_i^j, x^l(p_i + \Delta p_{ik})) g(x^l(p_i + \Delta p_{ik})), \quad (4)$$

where k indexes the sampled keys. p_i represents the 2-d spatial position of the query x_i^j in the feature map, and Δp_{ik} is the 2-d offset from the position p_i to the position of corresponding sampled key. As $p_i + \Delta p_{ik}$ can be fractional, bilinear interpolation is used as in [37] to compute $x(p_i + \Delta p_{ik})$. To further reduce the computational complexity in computing attention weights, we follow the design in Deformable DETR [38] to generate attention weights from query feature alone. Thus, our proposed CLA can be simplified as

$$y_i^j = \frac{1}{\mathcal{C}(x^j)} \sum_{l=1}^j \sum_{k=1}^K f(x_i^j) g(x^l(p_i + \Delta p_{ik})), \quad (5)$$

where f is the function to generate attention weights from the query feature. The structure of CLA is illustrated in Figure 1. Similar to the design for non-local attention module in [11], when deploying CLA in CNN backbones, we also wrap it into a non-local block with residual connection.

With our proposed CLA, each query feature from the input feature map refers to only a fixed number, K , of keys from each previous layer. However, query features at different spatial positions may have different preferences on keys sampled from different layers. The restoration process at different spatial positions may vary significantly due to

the diversity of textures in an image, especially for image restoration tasks. As a result, the number of most semantically similar keys at each layer may not be the same across different layers. Besides, when deploying CLA in CNN backbones for image restoration, we find that increasing the number of inserted CLA modules would not constantly improve the performance while incurring much higher inference cost. This observation motivates us to search for optimal insert positions of ACLA modules in neural networks to reduce the inference cost while maintaining competitive performance.

3.2 ACLA: Adaptive Cross-Layer Attention

To achieve adaptive key selection and the search for the optimal configuration of CLA, we propose Adaptive Cross-Layer Attention (ACLA). Specifically, for each query feature, we dynamically search for the keys sampled from previous layers with ACLA. Besides, when deploying ACLA in CNN backbones, a neural architecture search method is used to search for the insert positions of ACLA. An objective based on the inference cost of inserted ACLA modules is used to supervise the search procedure.

Adaptive Cross-Layer Attention. To adaptively search for the informative sampled keys for a query feature from its previous layers, we first follow the method in CLA to obtain a fixed number of sampled keys from each layer. Next, a hard gating mask is applied on each of the sampled keys as

$$y_i^j = \frac{1}{\mathcal{C}(x^j)} \sum_{l=1}^j \sum_{k=1}^K m_{i,k}^{j,l} f(x_i^j) g(x^l(p_i + \Delta p_{ik})), \quad (6)$$

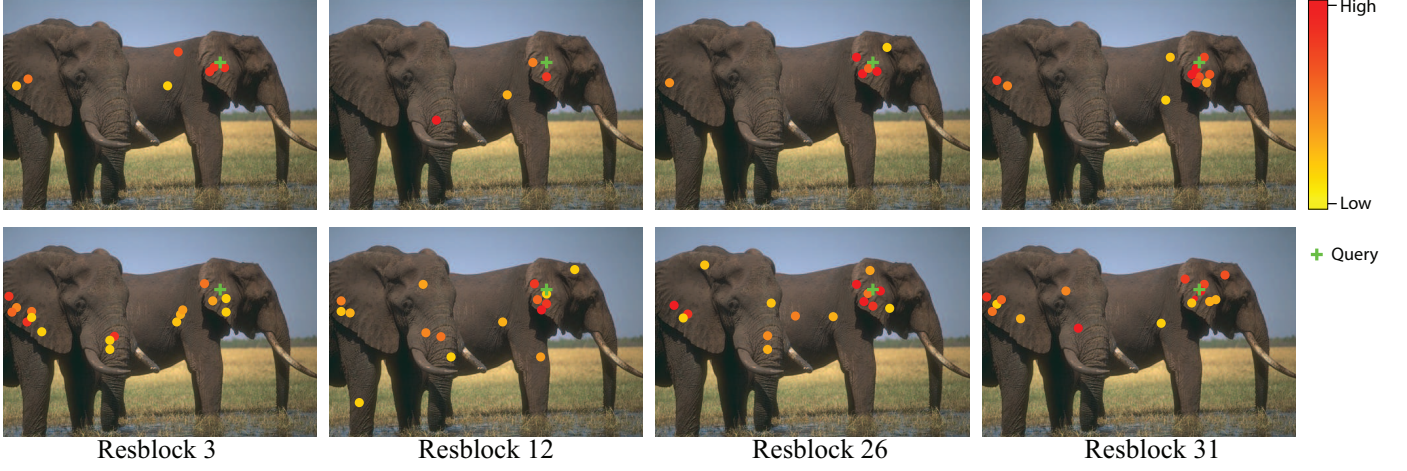


Fig. 2: Visualization of selected keys by ACLA for a query feature from the 31st resblock. The first row shows the positions of the keys selected by ACLA with $K = 16$. For comparison, the positions of keys with top-16 attention weights following the CLNL formulation in Equation (3) is displayed in the second row. From left to the right are the sampled key positions from the 3rd, 12nd, 26th, and 31st resblock. The query feature is shown as green cross marker. Each sampled key feature is marked as a circle whose color indicates its attention weight. It can be observed that ACLA adaptively selects semantically similar key features for the query feature, while its vanilla counterpart lacks such capability. More visualization results and analysis can be found in Section 4.8.

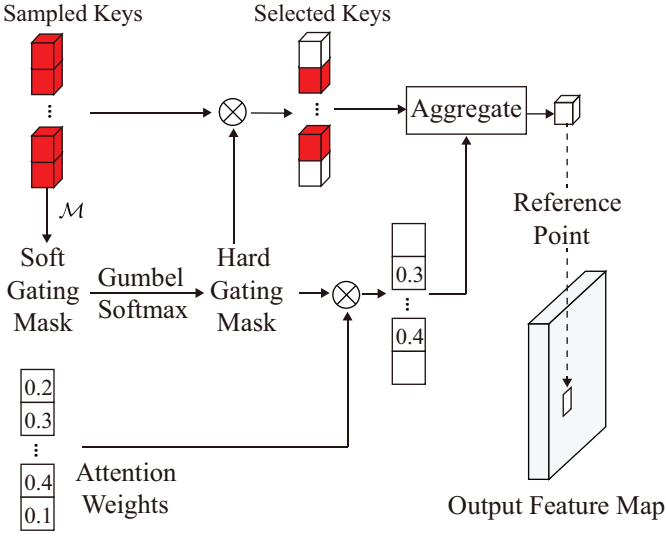


Fig. 3: Illustration of adaptive key selection in Adaptive Cross-Layer Attention (ACLA). The mask unit M generates a soft gating mask on the fixed number sampled keys, after which the Gumbel-Softmax turns the soft gating mask into a hard gating mask. The hard gating mask is applied on the features of the sampled keys and their corresponding attention weights before aggregation.

where $m_{i,k}^{j,l}$ is a binary hard gating mask for the k -th sampled key from x^l for query feature x_i^j , whose value is either 1 or 0. Compared to (5) for CLA, ACLA is more selective when aggregating key features to obtain the output feature. At layer l , it is expected that the most semantically

similar keys, which correspond to nonzero $m_{i,k}^{j,l}$, are used to generate the output feature.

To optimize the hard gating mask with gradient descent, we relax the hard gating mask into continuous domain with the simplified binary Gumbel-Softmax [39]. Thus, the hard gating mask $m_{i,k}^{j,l}$ can be approximated by

$$\hat{m}_{i,k}^{j,l} = \sigma \left(\frac{\beta_{i,k}^{j,l} + \epsilon_{i,k,1}^{j,l} - \epsilon_{i,k,2}^{j,l}}{\tau} \right), \quad (7)$$

where $\hat{m}_{i,k}^{j,l}$ is an approximation of the hard gating mask $m_{i,k}^{j,l}$ in continuous domain. $\beta_{i,k}^{j,l}$ is the sampling parameter. $\epsilon_{i,k,1}^{j,l}, \epsilon_{i,k,2}^{j,l}$ are Gumbel noise for the approximation. τ is the temperature, and σ is the Sigmoid function. During the training, the straight-through estimator from [39], [40] is used for $m_{i,k}^{j,l}$. In forward pass, the hard gating mask is computed by

$$m_{i,k}^{j,l} = \begin{cases} 1 & \hat{m}_{i,k}^{j,l} > 0.5, \\ 0 & \hat{m}_{i,k}^{j,l} \leq 0.5. \end{cases} \quad (8)$$

In the backward pass, we set $m_{i,k}^{j,l} = \hat{m}_{i,k}^{j,l}$ to enable the regular fractional gradient used in stochastic gradient descent.

The sampling parameter $\beta_{i,k}^{j,l}$ in Equation (7) can be regarded as a soft gating mask, which is used to generate the hard gating mask. To achieve input-dependent key selection, a mask unit M is used to generate the soft gating mask β from the features of the sampled keys as

$$\beta_{i,k}^{j,l} = M(x^l(p_i + \Delta p_{ik})). \quad (9)$$

Following the design in [39], a 1×1 convolution layer is used as the mask unit M in our model. Besides, Gumbel noise $\epsilon_{i,l,1}^k$ and $\epsilon_{i,l,2}^k$ are set to 0 during inference. With such design, we are able to generate a soft gating mask from features of sampled keys and turn it into a hard gating mask to achieve the search for sampled keys based on the input.

The adaptive key selection process of ACLA is illustrated in Figure 3. We would like to emphasize that while both CLA and ACLA have a parameter K , the meaning of this parameter is significantly different for each method. While CLA sample a fixed number, K , of keys at each layer, ACLA would only sample at most K keys at each layer. The number of sampled keys at layer by ACLA is determined by optimization of the neural network with ACLA modules, which includes the searching process for the informative sampled keys at each layer.

To demonstrate the effectiveness of adaptive key selection in ACLA, we compare the keys selected by ACLA and those selected by vanilla Cross-Layer Non-Local (CLNL) at different layers for a query feature in Figure 2. It can be observed that semantically similar keys are selected by ACLA for the query feature.

Insert Positions for ACLA. As demonstrated in Section 4.7, the positions where ACLA modules are inserted into the neural backbone have considerable effect in the final performance. In order to decide the insert positions of ACLA modules in a neural backbone, we propose the following search method. We first densely insert ACLA after each layer of the CNN backbone as shown in Figure 4 to build the supernet for the search. Similar to the gating formulation in ACLA, we define a hard decision parameter $s_j \in \{0, 1\}$ for the j -th inserted ACLA in the supernet. $s_j = 1$ indicates that an ACLA module is inserted after the j -th layer, and $s_j = 0$ otherwise. As a result, the output of ACLA in the supernet can be expressed as

$$y_i^j = \frac{1}{\mathcal{C}(x^j)} \sum_{l=1}^j s_l \sum_{k=1}^K m_{i,k}^{j,l} f(x_i^j) g(x^l(p_i + \Delta p_{ik})). \quad (10)$$

The simplified binary Gumbel-Softmax [39] is used here to approximate the hard decision parameter s_j by

$$\hat{s}_j = \sigma\left(\frac{\alpha_j + \epsilon_1^j - \epsilon_2^j}{\tau}\right), \quad (11)$$

with sampling parameter α_j , Gumbel noise ϵ , and temperature τ . Different from input-dependent design of the gating mask in ACLA, here we directly replace s_j with its continuous approximation \hat{s}_j . α_j here can be regarded as architecture parameter and can be directly optimized by stochastic gradient descent (SGD) during the search process. By gradually decreasing the temperature τ , α_j will be optimized such that s_j will approach 1 or 0.

Search Procedure. We need to optimize both the accuracy of a neural network and the inference cost (FLOPs) of the ACLA modules inserted into that neural network. Therefore, the inference cost of the ACLA modules inserted needs to be estimated during the search phase. Following the formulation of the ACLA in the supernet, the inference cost of the ACLA inserted after the j -th residual block as

$$\text{cost}_j = \sum_{l=1}^j s_l \sum_{k=1}^K (2m_{i,k}^{j,l} NC^2 + 2NC^2 + 6KNC), \quad (12)$$

where N is the number of spatial positions, C is the number of channels, K is the maximal number of sampled keys. $2m_{i,k}^{j,l} NC^2$ is the FLOPs for the convolution on generating the gating masks. $2NC^2 + 6KNC$ is the FLOPs for the generating the attention weights and 2-d offsets in (5). Then

we obtain the inference cost of all inserted ACLA modules as

$$\text{cost} = \sum_{j=1}^L s_j \text{cost}_j. \quad (13)$$

As mentioned before, due to relaxation to continuous problems, we search for the architecture of ACLA, which is comprised of sampled keys at each layer and the insert positions of ACLA modules, by updating the architecture parameters using SGD. The architecture parameters of ACLA are $\alpha = \{\alpha_j\}_{j=1}^L$, where L is the number of layers in the neural network with ACLA.

To supervise the search process, we design a loss function with the cost-based regularization to achieve the multi-objective optimization:

$$\mathcal{L}(w, \alpha) = \mathcal{L}_{MSE} + \lambda \log \text{cost}, \quad (14)$$

where λ is the hyper-parameters that controls the magnitude of the cost term.

We find that at the beginning of the search process, ACLA modules inserted at shallow layers are more likely to be maintained. Similar problem has been observed by previous NAS works [41]. To solve this problem, we follow DCNAS [41] and split our search procedure into two stages. In the first stage, we only optimize the parameters of the network for enough epochs to get network weights sufficiently trained. In the second stage, we activate the architecture optimization. We alternatively optimize the network weights by descending $\nabla_w \mathcal{L}_{train}(w, \alpha)$ on the training set, and optimize the architecture parameters by descending $\nabla_\alpha \mathcal{L}_{val}(w, \alpha)$ on the validation set. When the search procedure terminates, we derive the insert positions based on the architecture parameters α .

4 EXPERIMENTS

4.1 Implementation Details

We use DIV2K [42] as the training set for our experiments as like in previous works [16], [19]. DIV2K includes 800 images for training and 100 images for validation. We augment the training images by randomly rotating 90° , 180° , 270° , and horizontally flipping. In each mini-batch, 16 low-quality patches with size 48×48 are provided as inputs. ADAM optimizer is used for both the search phase and training phase. Default values of β_1 and β_2 are set to 0.9 and 0.999 respectively, and we set $\epsilon = 10^{-8}$. In the search phase, the learning rate is initialized as 10^{-4} , and cosine learning rate schedule is used. The search process takes 200 epochs. The first stage of search takes 100 epochs, and the second stage takes the remaining 100 epochs. In the training phase, the learning rate is initialized as 10^{-4} and then reduced to half for every 200 epochs. The model is trained for 1000 epochs in total. In our experiments with CLA, we manually insert four CLA modules evenly in the CNN backbones. The number of selected keys K is set to 8 for all CLA modules by default. For all ACLA modules, the maximum number of selected keys, which is also denoted by K , is initialized as 16. Before the search, we perform a cross-validation on 20% of the training data to decide the value of λ . Another 10% of training data is held for evaluation in the cross-validation process. The hyper-parameter λ is selected

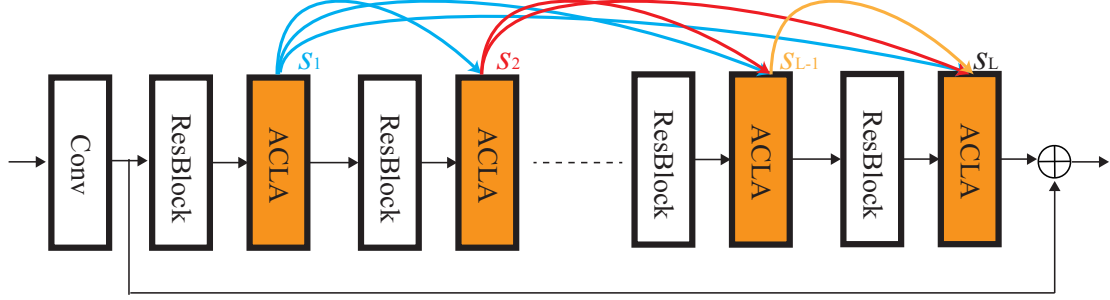


Fig. 4: Illustration of the search for insert positions in ACLA

from a candidate set $\{0.1, 0.15, 0.2, 0.25, 0.3, 0.35, 0.4\}$. The selected λ for different tasks are summarized in Table 18.

4.2 Single Image Super-Resolution

For single image super-resolution, we test our methods on top of the widely used super-resolution backbone EDSR [43] and RCAN [44]. The LR images are obtained by the bicubic downsampling of HR images. Our methods are evaluated on five standard datasets, Set5 [45], Set14 [46], B100 [47], Urban100 [48], and Manga109 [49]. The reconstructed results by our model are first converted to YCbCr space. PSNR and SSIM in the luminance channel is calculated in our experiments. We compare our methods with six baselines methods, SRCNN [50], VDSR [51], MemNet [6], SRMDNF [52], RDN [16], and HAN [12]. The quantitative results are shown in Table 1. Our methods greatly improve the performance of EDSR and RCAN on all benchmarks with all upsampling scales. Besides, our proposed ACLA outperforms the current state-of-the-art method HAN [12]. Although HAN is proposed to explore the interrelationship among features at different layers, it assigns a single importance weight to the feature map at each layer and neglects the difference of spatial positions. Such improvements demonstrate the superiority of the pixel-wise cross-layer attention design in our proposed CLA and ACLA.

4.3 Image Denoising

We also evaluate CLA and ACLA modules on standard benchmarks, KCLDAk24, BSD68 [47], and Urban100 [48], for image denoising. The noisy images are created by adding AWGN noises with $\sigma = 10, 30, 50, 70$. We compare our approach with four baseline methods, DnCNN [7], MemNet [6], RNAN [1], and PANet [20]. For fair comparisons, a 16-layer EDSR is used as the baseline CNN backbone, and CLA/ACLA modules are to be inserted into such neural backbone. We use PNSR as the metric to evaluate different methods. As shown in Table 2, our methods achieve remarkable improvements on the baseline EDSR on all benchmarks with all noise level. Besides, with less parameters, our models often outperform attention based methods RNAN and PANet, suggesting the superiority of CLA and ACLA. To verify that such improvement is statistically significant and out of the range of error, we train both ACLA and the previous SOTA method 10 times with different seeds for random initialization of the networks. Besides, we perform t-test between the results of ACLA and the results of the previous SOTA method on each test dataset to see if the improvement of ACLA is statistically significant. The results for single image super-resolution are displayed in Table 5. The comparison is performed between ACLA and HAN. We can see that ACLA consistently improves the PSNR results on different test datasets. The standard deviation of PSNR results on all test datasets is less than 0.001. The largest p-value is 0.0011 on Set 14, which is less than 0.05. This suggests that the improvement of ACLA over HAN is statistically significant

on each test dataset to see if the improvement of ACLA is statistically significant.

4.4 Image Compression Artifacts Reduction

For the task of image compression artifacts reduction (CAR), we compare our methods with DnCNN [7], RNAN [1], and PANet [20]. All methods are evaluated on LIVE1 [53] and Classic5 [54]. To obtain the low-quality compressed images, we follow the standard JPEG compression process and use the MATLAB JPEG encoder with quality $q = 10, 20, 30, 40$. For fair comparison, the results are only evaluated on the Y channel in the YCbCr Space. We also use PSNR as the metric to evaluate different methods. The results are shown in Table 3, where a 16-layer EDSR is used as the baseline CNN backbone. It can be observed that both CLA and ACLA boost the performance of the CNN backbone and surpass other baseline methods on all the benchmarks at different JPEG compression qualities.

4.5 Image Demosaicing

For the task of image demosaicing, the evaluation is conducted on Kodak24, McMaster [3], BSD68, and Urban100, following the settings in RNAN [1]. We compare our methods with IRCNN [3], RNAN [1], and PANet [20]. A 16-layer EDSR serves as the baseline CNN model. PSNR is used as the metric to evaluate different methods. As shown in Table 4, ACLA always yields the best reconstruction result for image demosaicing.

4.6 Improvement Significance Analysis

To verify that the improvement of our proposed ACLA on existing methods is statistically significant and out of the range of error, we train both ACLA and the previous SOTA method 10 times with different seeds for random initialization of the networks. Besides, we perform t-test between the results of ACLA and the results of the previous SOTA method on each test dataset to see if the improvement of ACLA is statistically significant. The results for single image super-resolution are displayed in Table 5. The comparison is performed between ACLA and HAN. We can see that ACLA consistently improves the PSNR results on different test datasets. The standard deviation of PSNR results on all test datasets is less than 0.001. The largest p-value is 0.0011 on Set 14, which is less than 0.05. This suggests that the improvement of ACLA over HAN is statistically significant

TABLE 1: Quantitative results on benchmark datasets for single image super-resolution

Method	Scale	Params(M)	Set5		Set14		B100		Urban100		Manga109	
			PSNR	SSIM								
Bicubic	$\times 2$	-	33.66	0.9299	30.24	0.8688	29.56	0.8431	26.88	0.8403	30.80	0.9339
SRCCNN	$\times 2$	0.244	36.66	0.9542	32.45	0.9067	31.36	0.8879	29.50	0.8946	35.60	0.9663
VDSR	$\times 2$	0.672	37.53	0.9590	33.05	0.9130	31.90	0.8960	30.77	0.9140	37.22	0.9750
MemNet	$\times 2$	0.677	37.78	0.9597	33.28	0.9142	32.08	0.8978	31.31	0.9195	37.72	0.9740
SRMDNF	$\times 2$	5.69	37.79	0.9601	33.32	0.9159	32.05	0.8985	31.33	0.9204	38.07	0.9761
RDN	$\times 2$	22.6	38.24	0.9614	34.01	0.9212	32.34	0.9017	32.89	0.9353	39.18	0.9780
HAN	$\times 2$	17.3	38.27	0.9614	34.16	0.9217	32.41	0.9027	33.35	0.9385	39.46	0.9787
EDSR	$\times 2$	40.7	38.11	0.9602	33.92	0.9195	32.32	0.9013	32.93	0.9351	39.10	0.9773
EDSR + NL	$\times 2$	43.6	38.15	0.9606	34.00	0.9203	32.37	0.9021	33.05	0.9360	39.21	0.9778
EDSR+CLA	$\times 2$	42.1	38.24	0.9613	34.08	0.9214	32.41	0.9028	33.28	0.9367	39.23	0.9780
EDSR+ACLA	$\times 2$	42.3	38.31	0.9617	34.10	0.9221	32.43	0.9030	33.35	0.9385	39.42	0.9787
RCAN	$\times 2$	15.3	38.27	0.9614	34.12	0.9216	32.41	0.9027	33.34	0.9384	39.44	0.9786
RCAN+NL	$\times 2$	17.4	38.27	0.9613	34.13	0.9217	32.43	0.9028	33.36	0.9386	39.45	0.9788
RCAN+CLA	$\times 2$	16.5	38.27	0.9615	34.14	0.9218	32.43	0.9030	33.34	0.9385	39.46	0.9785
RCAN+ACLA	$\times 2$	16.7	38.30	0.9615	34.15	0.9217	32.45	0.9029	33.39	0.9387	39.48	0.9789
Bicubic	$\times 3$	-	30.39	0.8682	27.55	0.7742	27.21	0.7385	24.46	0.7349	26.95	0.8556
SRCCNN	$\times 3$	0.244	32.75	0.9090	29.30	0.8215	28.41	0.7863	26.24	0.7989	30.48	0.9117
VDSR	$\times 3$	0.672	33.67	0.9210	29.78	0.8320	28.83	0.7990	27.14	0.8290	32.01	0.9340
MemNet	$\times 3$	0.677	34.09	0.9248	30.00	0.8350	28.96	0.8001	27.56	0.8376	32.51	0.9369
SRMDNF	$\times 3$	5.69	34.12	0.9254	30.04	0.8382	28.97	0.8025	27.57	0.8398	33.00	0.9403
RDN	$\times 3$	22.6	34.71	0.9296	30.57	0.8468	29.26	0.8093	28.80	0.8653	34.13	0.9484
HAN	$\times 3$	17.3	34.75	0.9299	30.67	0.8483	29.32	0.8110	29.10	0.8705	34.48	0.9500
EDSR	$\times 3$	40.7	34.65	0.9280	30.52	0.8462	29.25	0.8093	28.80	0.8653	34.17	0.9476
EDSR+NL	$\times 3$	43.6	34.70	0.9291	30.57	0.8470	29.26	0.8102	28.87	0.8670	34.22	0.9484
EDSR+CLA	$\times 3$	42.1	34.75	0.9297	30.66	0.8481	29.30	0.8113	29.05	0.8700	34.33	0.9492
EDSR+ACLA	$\times 3$	42.3	34.76	0.9303	30.69	0.8484	29.34	0.8115	29.12	0.8706	34.40	0.9498
RCAN	$\times 3$	15.3	34.74	0.9299	30.65	0.8482	29.32	0.8111	29.09	0.8702	34.44	0.9499
RCAN+NL	$\times 3$	17.4	34.74	0.9300	30.66	0.8483	29.32	0.8113	29.12	0.8704	34.45	0.9499
RCAN+CLA	$\times 3$	16.5	34.75	0.9301	30.67	0.8485	29.31	0.8114	29.11	0.8705	34.46	0.9499
RCAN+ACLA	$\times 3$	16.7	34.74	0.9304	30.68	0.8485	29.33	0.8115	29.14	0.8709	34.48	0.9503
Bicubic	$\times 4$	-	28.42	0.8104	26.00	0.7027	25.96	0.6675	23.14	0.6577	24.89	0.7866
SRCCNN	$\times 4$	0.244	30.48	0.8628	27.50	0.7513	26.90	0.7101	24.52	0.7221	27.58	0.8555
VDSR	$\times 4$	0.672	31.35	0.8830	28.02	0.7680	27.29	0.7026	25.18	0.7540	28.83	0.8870
MemNet	$\times 4$	0.677	31.74	0.8893	28.26	0.7723	27.40	0.7281	25.50	0.7630	29.42	0.8942
SRMDNF	$\times 4$	5.69	31.96	0.8925	28.35	0.7787	27.49	0.7337	25.68	0.7731	30.09	0.9024
RDN	$\times 4$	22.6	32.47	0.8990	28.81	0.7871	27.72	0.7419	26.61	0.8028	31.00	0.9151
HAN	$\times 4$	17.3	32.64	0.9002	28.90	0.7890	27.80	0.7442	26.85	0.8094	31.42	0.9177
EDSR	$\times 4$	40.7	32.46	0.8968	28.80	0.7876	27.71	0.7420	26.64	0.8033	31.02	0.9148
EDSR+NL	$\times 4$	43.6	32.53	0.8984	28.82	0.7877	27.74	0.7430	26.71	0.8069	31.19	0.9154
EDSR+CLA	$\times 4$	42.1	32.64	0.9001	28.83	0.7880	27.79	0.7435	26.79	0.8083	31.16	0.9159
EDSR+ACLA	$\times 4$	42.3	32.64	0.9003	28.88	0.7883	27.85	0.7443	26.87	0.8087	31.24	0.9174
RCAN	$\times 4$	15.3	32.63	0.9002	28.87	0.7889	27.77	0.7436	26.82	0.8087	31.22	0.9173
RCAN+NL	$\times 4$	17.4	32.64	0.9001	28.88	0.7889	27.79	0.7440	26.85	0.8087	31.26	0.9176
RCAN+CLA	$\times 4$	16.5	32.65	0.9002	28.88	0.7891	27.80	0.7441	26.86	0.8087	31.27	0.9177
RCAN+ACLA	$\times 4$	16.7	32.64	0.9002	28.90	0.7892	27.82	0.7445	26.89	0.8089	31.29	0.9179

TABLE 2: Quantitative results on benchmark datasets for single image denoising

Method	Params (M)	KCLDAK24				BSD68				Urban100			
		10	30	50	70	10	30	50	70	10	30	50	70
MemNet	0.677	N/A	29.67	27.65	26.40	N/A	28.39	26.33	25.08	N/A	28.93	26.53	24.93
DnCNN	0.672	36.98	31.39	29.16	27.64	36.31	30.40	28.01	26.56	36.21	30.28	28.16	26.17
RNAN	7.409	37.24	31.86	29.58	28.16	36.43	30.63	28.27	26.83	36.59	31.50	29.08	27.45
PANet	5.957	37.35	31.96	29.65	28.20	36.50	30.70	28.33	26.89	36.80	31.87	29.47	27.87
baseline	5.430	37.21	31.85	29.60	28.15	36.34	30.60	28.28	26.84	36.63	31.64	29.22	27.54
NL	6.135	37.29	31.90	29.64	28.19	36.43	30.67	28.31	26.89	36.69	31.74	29.30	27.70
CLA	5.896	37.37	31.97	29.67	28.23	36.52	30.74	28.35	26.91	36.79	31.85	29.43	27.88
ACLA	5.914	37.38	31.97	29.70	28.25	36.54	30.77	28.36	26.94	36.85	31.90	29.49	27.91

with $p \ll 0.05$ and it is not caused by random error. For image denoising, image compression artifacts reduction, and image demosaicing, we compare ACLA with the previous SOTA, PANet. The results are shown in Table 6, Table 7, and Table 8 respectively. We can see that ACLA consistently improves the performance on different test datasets. The p-value for all these three tasks is less than 0.05, suggesting the statistically significant improvement of ACLA over PANet.

4.7 Ablation Study and Discussion

4.7.1 ACLA vs. Non-Local Attention

To verify the effectiveness of our proposed methods, we compare CLA and ACLA with Non-Local (NL) attention [11] and vanilla Cross-Layer Non-Local (CLNL) attention

TABLE 3: Quantitative results on benchmark datasets for image compression artifacts reduction

Method	Params (M)	LIVE1				Classic5			
		10	20	30	40	10	20	30	40
JPEG	-	27.77	30.07	31.41	32.35	27.82	30.12	31.48	32.43
DnCNN	0.672	29.19	31.59	32.98	33.96	29.40	31.63	32.91	33.77
RNAN	7.409	29.63	32.03	33.45	34.47	29.96	32.11	33.38	34.27
PANet	5.957	29.69	32.10	33.55	34.55	30.03	32.36	33.53	34.38
baseline	5.430	29.63	32.04	33.50	35.51	29.99	32.22	33.43	34.31
NL	6.135	29.65	32.08	33.55	35.53	30.03	32.34	33.51	34.41
CLA	5.896	29.73	32.13	33.57	35.54	30.05	32.38	33.55	34.42
ACLA	5.914	29.73	32.17	33.63	35.55	30.07	32.42	33.58	34.44

TABLE 4: Quantitative results on benchmark datasets for image demosaicing

Method	Params(M)	McMaster18		Kodak24		BSD68		Urban100	
		PSNR	SSIM	PSNR	SSIM	PSNR	SSIM	PSNR	SSIM
Mosaiced	-	9.17	0.1674	8.56	0.0682	8.43	0.0850	7.48	0.1195
IRCNN	0.731	37.47	0.9615	40.41	0.9807	39.96	0.9850	36.64	0.9743
RNAN	7.409	39.71	0.9725	43.09	0.9902	42.50	0.9929	39.75	0.9848
PANet	5.957	40.00	0.9737	43.29	0.9905	42.86	0.9933	40.50	0.9854
Baseline	5.430	39.81	0.9730	43.18	0.9903	42.66	0.9931	40.23	0.9852
NL	6.135	39.90	0.9732	43.23	0.9903	42.79	0.9932	40.39	0.9853
CLA	5.896	40.03	0.9739	43.35	0.9906	42.88	0.9934	40.52	0.9853
ACLA	5.914	40.08	0.9742	43.38	0.9908	42.90	0.9936	40.55	0.9857

TABLE 5: PSNR (mean/std) results comparison with p-value between ACLA and HAN for single-image super-resolution

Methdos	Scale	Set 5	Set 14	B100	Urban100	Manga109
HAN	$\times 2$	38.267 / 0.0025	34.147 / 0.0034	32.414 / 0.0049	33.344 / 0.0063	39.453 / 0.0061
ACLA	$\times 2$	38.303 / 0.0027	34.153 / 0.0047	32.449 / 0.0053	33.391 / 0.0070	39.479 / 0.0074
p-value	$\times 2$	8.58e-12	0.0011	1.94e-11	1.54e-08	0.0001
HAN	$\times 3$	34.745 / 0.0031	30.668 / 0.0033	29.319 / 0.0061	29.104 / 0.0059	34.477 / 0.0073
ACLA	$\times 3$	34.754 / 0.0027	30.682 / 0.0041	29.331 / 0.0049	29.139 / 0.0070	34.483 / 0.0045
p-value	$\times 3$	0.0013	2.45e-9	1.75e-7	3.12e-11	0.0004
HAN	$\times 4$	32.639 / 0.0023	28.898 / 0.0027	27.803 / 0.0057	26.852 / 0.0070	31.316 / 0.0089
ACLA	$\times 4$	32.644 / 0.0021	28.903 / 0.0037	27.820 / 0.0069	26.892 / 0.0091	31.297 / 0.0091
p-value	$\times 4$	0.0009	0.0017	3.12e-5	1.15e-13	1.97e-7

TABLE 6: PSNR (mean/std) results comparison with p-value between ACLA and PANet for image denoising

Methdos	σ	KCLDAK24	BSD68	Urban100
PANet	10	37.347 / 0.0076	36.503 / 0.0077	36.804 / 0.0082
ACLA	10	37.401 / 0.0069	36.572 / 0.0090	36.849 / 0.0088
p-value	10	3.75e-11	2.56e-10	5.67e-9
PANet	30	31.960 / 0.0059	30.704 / 0.0061	31.871 / 0.0073
ACLA	30	31.974 / 0.0060	30.758 / 0.0078	31.920 / 0.0097
p-value	30	1.48e-5	3.54e-9	2.13e-10
PANet	50	29.651 / 0.0053	28.333 / 0.0084	29.471 / 0.0069
ACLA	50	31.721 / 0.0076	28.384 / 0.0091	29.518 / 0.0085
p-value	50	3.85e-11	2.39e-12	1.97e-10
PANet	70	28.204 / 0.0079	26.894 / 0.0084	27.867 / 0.0062
ACLA	70	28.254 / 0.0081	26.944 / 0.0082	27.914 / 0.0080
p-value	70	2.73e-11	4e-11	1.5e-11

in terms of computational efficiency and performance. The CLNL follows the formulation in equation (3). The comparison is performed on Set5 for single image super-resolution with EDSR backbone. The NL and CLNL modules are inserted evenly after every 8th residual blocks. All the FLOPs in our ablation study are calculated for input size of 48×48 . Results are presented in Table 9. It can be observed that, with less computation cost, CLA and ACLA achieve much better performance compared to standard NL and CLNL modules.

4.7.2 ACLA vs. State-of-the-arts Attention Modules

In this subsection, we compare ACLA with several state-of-the-arts attention modules that are widely used in the CV community, including Squeeze-and-Excitation (SE) [23]

attention and Multi-Head Attention (MHA) [55]. SE models interdependencies between the channels of the convolutional features by reweighting the channel-wise responses using soft self-attention. MHA is in fact a variant of self-attention from the NLP domain. Specifically, MHA can be regarded as a special non-local attention that takes account of the relative position information. We insert four SE blocks and four MHA blocks evenly to the EDSR backbone, forming the baseline methods EDSR + SE and EDSR + MHA respectively in Table 10. The comparison is performed for $2 \times$ single-image super-resolution. The comparative results are shown in Table 10. Although MHA and SE bring improvements over the EDSR baseline, the best results are achieved by our proposed ACLA. Furthermore, we achieve even better performance by inserting a SE block after each ACLA module, as shown in the last row of Table 10.

4.7.3 Number of Selected keys K

As discussed in Section 3.1, CLA selects a fixed number of keys, that is K , at each layer for non-local attention. To verify that a small K is sufficient for competitive performance, we perform experiments on CLA with different value of K . The comparison is performed on Set5 ($\times 2$) for single image super-resolution with EDSR backbone. We also compare ACLA with different values of K , which is the maximal number of sampled keys. The results are shown in Table 11 and Table 12. With increased K , the performance of CLA and ACLA does not constantly improve. CLA with $K = 8$

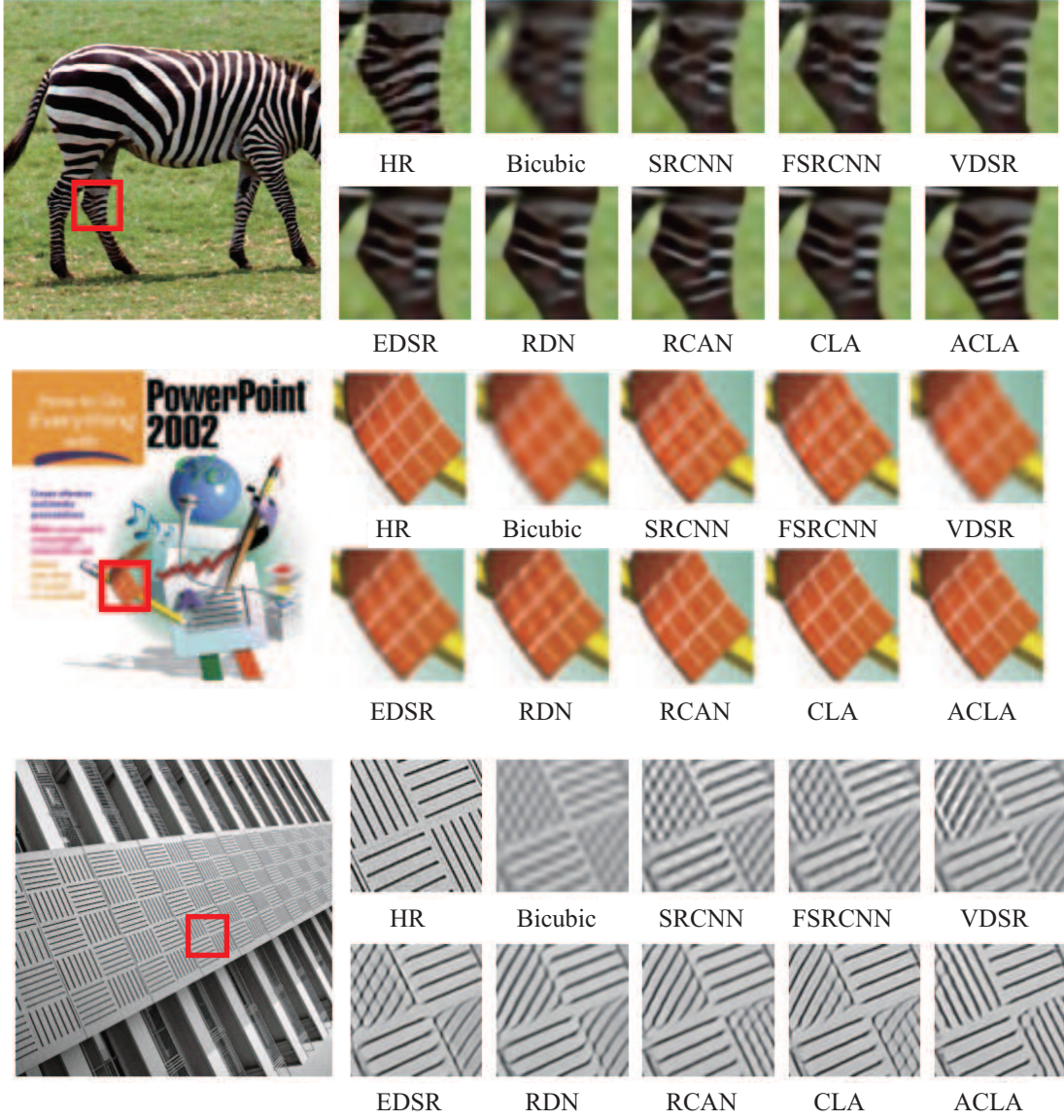


Fig. 5: Visual comparison for 4x SR with BI degradation model.

TABLE 7: PSNR (mean/std) results comparison with p-value between ACLA and PANet for image compression artifacts reduction

Method	q	LIVE1	Classic5	LIVE1	Classic5	LIVE1	Classic5	LIVE1	Classic5
PANet	10	29.688 / 0.0067	30.028 / 0.0130	29.688 / 0.0067	30.028 / 0.0130	29.688 / 0.0067	30.028 / 0.0130	29.688 / 0.0067	30.028 / 0.0130
ACLA	10	29.734 / 0.0085	30.073 / 0.0098	29.734 / 0.0085	30.073 / 0.0098	29.734 / 0.0085	30.073 / 0.0098	29.734 / 0.0085	30.073 / 0.0098
p-value	10	6.43e-11	7.05e-8	6.43e-11	7.05e-8	6.43e-11	7.05e-8	6.43e-11	7.05e-8

TABLE 8: PSNR (mean/std) results comparison with p-value between ACLA and PANet for image demosaicing

Method	McMaster18	Kodak24	BSD68	Urban100
PANet	40.004 / 0.0090	43.286 / 0.0118	42.857 / 0.0095	40.504 / 0.0112
ACLA	40.079 / 0.0125	43.374 / 0.0120	42.907 / 0.0102	40.557 / 0.0114
p-value	8.51e-12	4.85e-12	4.26e-9	4.83e-9

TABLE 9: Efficiency comparison with Non-Local attention on Set5

Method	PSNR	FLOPs(G)	Params(M)
EDSR	38.11	93.97	40.73
NL	38.15	109.38	43.56
CLNL	38.14	122.67	45.87
CLA (Ours)	<u>38.24</u>	96.93	42.13
ACLA (Ours)	<u>38.31</u>	96.97	42.29

and ACLA with $K = 16$ can already achieve comparable performance to those with larger K . This is also consistent with previous studies [56], [57] on the power of sparse representation learning for image restoration.

4.7.4 Insert Positions of CLA Modules

As stated in section 3.1, the inference cost of CLA is quadratic to the number of inserted CLA modules. To study the influence of the number of inserted modules N_{CLA} on the performance of CLA, we perform an ablation study on Set5 ($\times 2$) for single image super-resolution. We use EDSR with 32 layers as our backbone, where N_{CLA} CLA modules are evenly inserted after every $32/N_{\text{CLA}}$ layers. As shown in Table 13, when $N_{\text{CLA}} \geq 16$, an increased N_{CLA} does not

TABLE 10: Efficiency and performance comparison with Squeeze-and-Excitation (SE) attention and Multi-Head Attention (MHA)

Methods	Params(M)	FLOPs(G)	Set 5	Set 14	B 100	Urban 100	Manga 100
EDSR	40.73	93.97	38.11	33.92	32.32	32.93	39.10
EDSR + MHA	42.17	100.21	38.23	34.01	32.39	33.07	39.29
EDSR + SE	41.79	96.14	38.19	34.03	32.36	33.06	39.22
EDSR + ACLA	42.29	96.97	38.31	34.10	32.43	33.35	39.42
EDSR + ACLA + SE	43.47	99.32	38.33	34.09	32.44	33.38	39.46

TABLE 11: Ablation study on number of sampled keys in CLA on Set5

Method	K	PSNR	FLOPs(G)	Params(M)
CLA	4	38.22	96.71	42.09
CLA	8	38.24	96.93	42.13
CLA	16	38.25	97.38	42.21
CLA	32	38.23	97.90	42.39
CLA	64	38.25	98.92	42.74
CLA	128	38.24	100.32	43.37

TABLE 12: Ablation study on number of sampled keys in ACLA on Set5

Method	K	PSNR	FLOPs(G)	Params(M)
ACLA	8	38.28	96.78	42.18
ACLA	16	38.31	96.98	42.29
ACLA	32	38.30	97.56	42.41
ACLA	64	38.31	98.03	42.69
ACLA	128	38.29	99.17	43.02
ACLA	256	38.29	100.59	43.97

boost the performance while increasing the parameter size and the inference cost of the model. Such observation implies the necessity of searching for optimal insert positions of CLA modules, and this also motivates us to search for the optimal insert positions of ACLA.

TABLE 13: Ablation study on number of inserted CLA modules on Set5

Method	N_{CLA}	PSNR	FLOPs(G)	Params(M)
CLA	2	38.20	94.79	41.24
CLA	4	38.24	96.93	42.13
CLA	8	38.27	101.37	44.35
CLA	16	38.27	118.48	51.47
CLA	24	38.26	139.63	62.89
CLA	32	38.26	182.93	79.29

4.7.5 Ablation Study on ACLA

In Section 3.2, two adaptive designs are proposed and applied in our ACLA module. The first adaptive design is to select an adaptive number of keys at each layer for non-local attention, and the second adaptive design is to search for optimal insert positions of ACLA modules. To verify the effectiveness of these two adaptive designs in ACLA, we designed two baseline modules, CLA-I and CLA-K. CLA-I stands for CLA with the search for insert positions as that in ACLA. CLA-K stands for CLA which selects an adaptive number of keys at each layer, as that in ACLA.

We perform an ablation study with comparison between ACLA, CLA-I, CLA-K, and CLA. The comparison is performed on Set5 ($\times 2$) for single image super-resolution

with EDSR backbone. The comparative results are shown in Table 14. It can be observed that each adaptive design improves the original CLA. ACLA, as a combination of the two adaptive designs, renders better performance than each individual adaptive design.

TABLE 14: Ablation study on the effectiveness of insertion position search and adaptive key selection

Method	PSNR	FLOPs(G)	Params(M)
CLA	38.24	96.93	42.13
CLA-I	38.27	96.93	42.13
CLA-K	38.28	96.87	42.29
ACLA	38.31	96.98	42.29

4.7.6 Ablation study on the number of referred layers in CLA and ACLA

We perform an ablation study on the number of referred layers in 2x single-image super-resolution to verify the effectiveness of referring key pixels from previous CNN layers. We use EDSR as our backbone and all experiment settings are the same as reported in Section 4 in our paper. The results for CLA is displayed in Table 15. Because only 4 CLA modules are inserted in EDSR + CLA, CLA with 4 referred layers is the same as the EDSR+CLA reported in Table 1 of our paper. In CLA with i referred layers ($1 \leq i \leq 5$), each CLA module only refers to the last i layers with CLA modules. When $i = 1$, CLA with 1 referred layer only refers to keys from the same layer, so it is the same as NL (the classical non-local module). Same ablation study is also performed for EDSR + ACLA. Since 5 ACLA modules are inserted in EDSR + ACLA, ACLA with 5 referred layers is the same as the EDSR+ACLA reported in Table 16. From the results shown below, we can clearly see the benefits of referring key pixels from previous CNN layers.

TABLE 15: Ablation study on the number of referred layers in CLA

Methods	Layers	Set 5	Set 14	B100	Urban100	Manga109
EDSR	-	38.11	33.92	32.32	32.93	39.10
CLA	1	38.16	34.00	32.35	33.03	39.17
CLA	2	38.18	34.04	32.37	33.11	39.20
CLA	3	38.23	34.06	32.41	33.26	39.23
CLA	4	38.24	34.08	32.41	33.28	39.23

TABLE 16: Ablation study on the number of referred layers in ACLA

Methods	Layers	Set 5	Set 14	B100	Urban100	Manga109
EDSR	-	38.11	33.92	32.32	32.93	39.10
ACLA	1	38.19	34.02	32.35	33.09	39.18
ACLA	2	38.23	34.03	32.36	33.14	39.23
ACLA	3	38.26	34.07	32.41	33.27	39.34
ACLA	4	38.25	34.07	32.44	33.32	39.38
ACLA	5	38.31	34.10	32.45	33.35	39.42

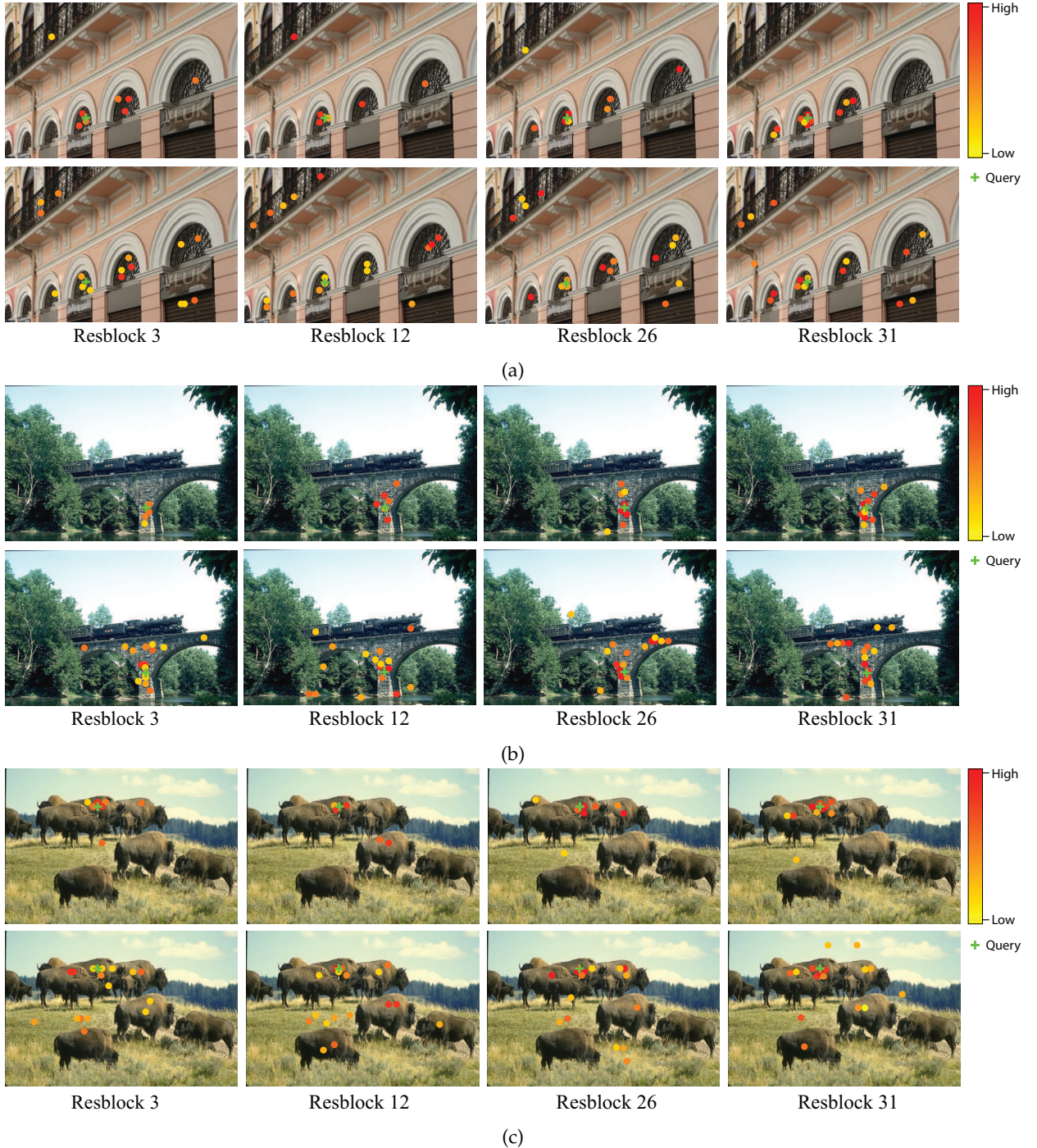


Fig. 6: Visualization of selected keys by ACLA

4.7.7 Inference Time Comparison

We compare the inference time between our proposed ACLA and previous state-of-the-arts methods. The running time is the average of 1000 runs on input of size 48×48 . We evaluate the running time on a single Tesla V100 16G. We compare our proposed methods with HAN [12] and SAN [19], which are also attention-based methods for single image super-resolution. As shown in the Table 17, EDSR+ACLA achieves better performance than HAN with much less inference time.

TABLE 17: Inference time comparison

	RCAN	HAN	SAN	RCAN+ACLA	EDSR+ACLA
Set 5 (PSNR)	38.27	38.27	38.31	38.30	38.31
Time(ms)	32.7	38.9	61.2	36.9	19.8

4.7.8 Analysis on Search Results

We summarize the value of λ , i.e. hyper-parameter that controls the magnitude of the inference cost term, for different tasks in Table 18. The insert positions of ACLA in the searched models are also shown in the same table. Since RCAN constitutes 10 residual groups, we insert ACLA mod-

ule after each residual group in the corresponding super network. For experiments with EDSR, ACLA modules are inserted after each residual block in the super network. Note that 16-layer EDSR is used for image super-resolution, image denoising, image demosaicing, and image compression artifacts reduction.

TABLE 18: Search settings for ACLA in different experiments

Task	Backbone	Value of λ	Insert Positions
Super-Resolution	EDSR	0.15	3, 12, 26, 31, 32
Super-Resolution	RCAN	0.3	1, 3, 5, 9
Denoising	EDSR	0.35	2, 7, 9, 13, 15
Demosaicing	EDSR	0.3	2, 5, 11, 14, 16
Artifacts Reduction	EDSR	0.35	2, 7, 10, 13, 14

4.8 Visualization of Selected Keys

We present more examples on visualization of selected keys by ACLA in Figure 6 to demonstrate the superiority of our method in searching for informative keys for query feature. The visualization is based on our results for $2\times$ image super-resolution. Similar to Figure 2, the first row shows the positions of the keys selected by ACLA with $K = 16$. For comparison, the positions of keys with top-16 attention weights following the vanilla CLNL attention formulation in Equation (3) is displayed in the second row. From left to the right are the sampled key positions from the 3rd, 12nd, 26th, and 31st resblock.

The visualization results show that ACLA adaptively selects semantically similar keys for the query feature, and its vanilla counterpart CLNL lacks such capability. For instance, in Figure 2, the query is from the ear of the elephant on the right side. With ACLA, 60% of the selected keys across are also from the ear of the same elephant. Besides, among the keys selected outside the ear of the same elephant, 5 out of 11 are from the ear of the elephant on the left, which have similar textures as the ear of the elephant on the right. While with CLNL, only 39% of the selected keys are from the ear of the elephant on the right. Similar observations can also be found in Figure 6. In Figure 6 (a), we pick a query point from the frame structure at the top of a gate. With ACLA, 90% of the keys selected are distributed on the frame structures at the top of gates. While with CLNL, positions from the gates and the frame structure at the balcony are also given high attention weights. Only 61% of the selected keys are distributed on the frame structures at the top of gates, which may limit the power of attention modules. Similar observations can also be found Figure 6 (b) and Figure 6 (c). In Figure 6 (b), the query is from the bridge in the middle of the image. All the keys selected by ACLA are also from the bridge. In Figure 6 (c), the query is from the back of a yak. Most of the keys selected by ACLA are also located on the body of yaks. While as shown in the second row, CLNL even assigns large attention weights to positions from the grass and the background. Such observations strongly demonstrate the power of ACLA in searching for informative keys across different layers.

5 CONCLUSIONS

In this paper, we first propose a novel non-local attention module termed Cross-Layer Attention (CLA), which searches for informative keys across different layers for each query feature. We further propose Adaptive CLA, or ACLA, which improves CLA by two adaptive designs: selecting adaptive number of keys at each layer and searching for insert positions of ACLA modules. In particular, each query feature selects adaptive keys at layer layers. A search method is used to search for the insert positions of ACLA modules so that the neural network with ACLA modules is compact with competitive performance. Experiments on image restoration tasks including single-image super resolution, image denoising, image compression artifacts reduction, and image demosaicing validate the effectiveness and efficiency of the proposed CLA and ACLA.

REFERENCES

- [1] Y. Zhang, K. Li, K. Li, B. Zhong, and Y. Fu, "Residual non-local attention networks for image restoration," in *International Conference on Learning Representations*, 2019.
- [2] D. Liu, B. Wen, Y. Fan, C. C. Loy, and T. S. Huang, "Non-local recurrent network for image restoration," in *Advances in Neural Information Processing Systems*, 2018, pp. 1673–1682.
- [3] K. Zhang, W. Zuo, S. Gu, and L. Zhang, "Learning deep cnn denoiser prior for image restoration," in *CVPR*, 2017.
- [4] Y. Fan, J. Yu, D. Liu, and T. S. Huang, "Scale-wise convolution for image restoration," *arXiv preprint arXiv:1912.09028*, 2019.
- [5] W.-S. Lai, J.-B. Huang, N. Ahuja, and M.-H. Yang, "Deep laplacian pyramid networks for fast and accurate super-resolution," in *CVPR*, 2017.
- [6] Y. Tai, J. Yang, X. Liu, and C. Xu, "Memnet: A persistent memory network for image restoration," in *Proceedings of the IEEE international conference on computer vision*, 2017, pp. 4539–4547.
- [7] K. Zhang, W. Zuo, Y. Chen, D. Meng, and L. Zhang, "Beyond a gaussian denoiser: Residual learning of deep cnn for image denoising," *TIP*, 2017.
- [8] A. Buades, B. Coll, and J.-M. Morel, "A non-local algorithm for image denoising," in *CVPR*, 2005.
- [9] D. Zoran and Y. Weiss, "From learning models of natural image patches to whole image restoration," in *2011 International Conference on Computer Vision*. IEEE, 2011, pp. 479–486.
- [10] M. Zontak, I. Mosseri, and M. Irani, "Separating signal from noise using patch recurrence across scales," in *Proceedings of the IEEE Conference on Computer Vision and Pattern Recognition*, 2013, pp. 1195–1202.
- [11] X. Wang, R. Girshick, A. Gupta, and K. He, "Non-local neural networks," in *Proceedings of the IEEE conference on computer vision and pattern recognition*, 2018, pp. 7794–7803.
- [12] B. Niu, W. Wen, W. Ren, X. Zhang, L. Yang, S. Wang, K. Zhang, X. Cao, and H. Shen, "Single image super-resolution via a holistic attention network," in *European Conference on Computer Vision*. Springer, 2020, pp. 191–207.
- [13] Y. Tay, M. Dehghani, V. Aribandi, J. Gupta, P. Pham, Z. Qin, D. Bahri, D.-C. Juan, and D. Metzler, "Omniinet: Omnidirectional representations from transformers," *arXiv preprint arXiv:2103.01075*, 2021.
- [14] B. Lim, S. Son, H. Kim, S. Nah, and K. M. Lee, "Enhanced deep residual networks for single image super-resolution," in *The IEEE Conference on Computer Vision and Pattern Recognition (CVPR) Workshops*, July 2017.
- [15] C. Dong, Y. Deng, C. Change Loy, and X. Tang, "Compression artifacts reduction by a deep convolutional network," in *ICCV*, 2015.
- [16] Y. Zhang, Y. Tian, Y. Kong, B. Zhong, and Y. Fu, "Residual dense network for image super-resolution," in *Proceedings of the IEEE conference on computer vision and pattern recognition*, 2018, pp. 2472–2481.
- [17] M. Haris, G. Shakhnarovich, and N. Ukita, "Deep back-projection networks for super-resolution," in *Proceedings of the IEEE conference on computer vision and pattern recognition*, 2018, pp. 1664–1673.

[18] N. Ahn, B. Kang, and K.-A. Sohn, "Fast, accurate, and lightweight super-resolution with cascading residual network," in *Proceedings of the European Conference on Computer Vision (ECCV)*, 2018, pp. 252–268.

[19] T. Dai, J. Cai, Y. Zhang, S.-T. Xia, and L. Zhang, "Second-order attention network for single image super-resolution," in *Proceedings of the IEEE conference on computer vision and pattern recognition*, 2019, pp. 11 065–11 074.

[20] Y. Mei, Y. Fan, Y. Zhang, J. Yu, Y. Zhou, D. Liu, Y. Fu, T. S. Huang, and H. Shi, "Pyramid attention networks for image restoration," *arXiv preprint arXiv:2004.13824*, 2020.

[21] K. Xu, J. Ba, R. Kiros, K. Cho, A. Courville, R. Salakhudinov, R. Zemel, and Y. Bengio, "Show, attend and tell: Neural image caption generation with visual attention," in *International conference on machine learning*. PMLR, 2015, pp. 2048–2057.

[22] L. Chen, H. Zhang, J. Xiao, L. Nie, J. Shao, W. Liu, and T.-S. Chua, "Sca-cnn: Spatial and channel-wise attention in convolutional networks for image captioning," in *Proceedings of the IEEE conference on computer vision and pattern recognition*, 2017, pp. 5659–5667.

[23] J. Hu, L. Shen, and G. Sun, "Squeeze-and-excitation networks," in *Proceedings of the IEEE conference on computer vision and pattern recognition*, 2018, pp. 7132–7141.

[24] F. Wang, M. Jiang, C. Qian, S. Yang, C. Li, H. Zhang, X. Wang, and X. Tang, "Residual attention network for image classification," in *Proceedings of the IEEE conference on computer vision and pattern recognition*, 2017, pp. 3156–3164.

[25] Y. Zhang, K. Li, K. Li, L. Wang, B. Zhong, and Y. Fu, "Image super-resolution using very deep residual channel attention networks," in *Proceedings of the European Conference on Computer Vision (ECCV)*, 2018, pp. 286–301.

[26] H. Chen, Y. Wang, T. Guo, C. Xu, Y. Deng, Z. Liu, S. Ma, C. Xu, C. Xu, and W. Gao, "Pre-trained image processing transformer," in *Proceedings of the IEEE/CVF Conference on Computer Vision and Pattern Recognition*, 2021, pp. 12 299–12 310.

[27] J. Liang, J. Cao, G. Sun, K. Zhang, L. Van Gool, and R. Timofte, "Swinir: Image restoration using swin transformer," *arXiv preprint arXiv:2108.10257*, 2021.

[28] B. Zoph and Q. V. Le, "Neural architecture search with reinforcement learning," in *International Conference on Learning Representations (ICLR)*, 2016.

[29] L. Xie and A. Yuille, "Genetic cnn," in *Proceedings of the IEEE/CVF International Conference on Computer Vision (ICCV)*, 2017.

[30] H. Pham, M. Guan, B. Zoph, Q. Le, and J. Dean, "Efficient neural architecture search via parameters sharing," in *International Conference on Machine Learning (ICML)*, 2018.

[31] C. Liu, B. Zoph, M. Neumann, J. Shlens, W. Hua, L.-J. Li, L. Fei-Fei, A. Yuille, J. Huang, and K. Murphy, "Progressive neural architecture search," in *Proceedings of the European conference on computer vision (ECCV)*, 2018, pp. 19–34.

[32] H. Liu, K. Simonyan, and Y. Yang, "Darts: Differentiable architecture search," in *International Conference on Learning Representations (ICLR)*, 2018.

[33] S. Xie, H. Zheng, C. Liu, and L. Lin, "Snas: stochastic neural architecture search," in *International Conference on Learning Representations (ICLR)*, 2018.

[34] C. Liu, L.-C. Chen, F. Schroff, H. Adam, W. Hua, A. L. Yuille, and L. Fei-Fei, "Auto-deeplab: Hierarchical neural architecture search for semantic image segmentation," in *Proceedings of the IEEE/CVF Conference on Computer Vision and Pattern Recognition (CVPR)*, 2019.

[35] X. Zhang, H. Xu, H. Mo, J. Tan, C. Yang, L. Wang, and W. Ren, "Dcnas: Densely connected neural architecture search for semantic image segmentation," in *Proceedings of the IEEE/CVF Conference on Computer Vision and Pattern Recognition*, 2021, pp. 13 956–13 967.

[36] Y. Guo, Y. Luo, Z. He, J. Huang, and J. Chen, "Hierarchical neural architecture search for single image super-resolution," *IEEE Signal Processing Letters*, vol. 27, pp. 1255–1259, 2020.

[37] J. Dai, H. Qi, Y. Xiong, Y. Li, G. Zhang, H. Hu, and Y. Wei, "Deformable convolutional networks," in *Proceedings of the IEEE international conference on computer vision*, 2017, pp. 764–773.

[38] X. Zhu, W. Su, L. Lu, B. Li, X. Wang, and J. Dai, "Deformable detr: Deformable transformers for end-to-end object detection," *arXiv preprint arXiv:2010.04159*, 2020.

[39] T. Verelst and T. Tuytelaars, "Dynamic convolutions: Exploiting spatial sparsity for faster inference," in *Proceedings of the IEEE/CVF Conference on Computer Vision and Pattern Recognition*, 2020, pp. 2320–2329.

[40] Y. Bengio, N. Léonard, and A. Courville, "Estimating or Propagating Gradients Through Stochastic Neurons for Conditional Computation," 8 2013. [Online]. Available: <http://arxiv.org/abs/1308.3432>

[41] J. Fang, Y. Sun, Q. Zhang, Y. Li, W. Liu, and X. Wang, "Densely connected search space for more flexible neural architecture search," in *Proceedings of the IEEE/CVF Conference on Computer Vision and Pattern Recognition*, 2020, pp. 10 628–10 637.

[42] R. Timofte, E. Agustsson, L. Van Gool, M.-H. Yang, and L. Zhang, "Ntire 2017 challenge on single image super-resolution: Methods and results," in *Proceedings of the IEEE conference on computer vision and pattern recognition workshops*, 2017, pp. 114–125.

[43] B. Lim, S. Son, H. Kim, S. Nah, and K. Mu Lee, "Enhanced deep residual networks for single image super-resolution," in *Proceedings of the IEEE conference on computer vision and pattern recognition workshops*, 2017, pp. 136–144.

[44] Y. Zhang, K. Li, K. Li, L. Wang, B. Zhong, and Y. Fu, "Image super-resolution using very deep residual channel attention networks," in *Proceedings of the European Conference on Computer Vision (ECCV)*, 2018, pp. 286–301.

[45] M. Bevilacqua, A. Roumy, C. Guillemot, and M. L. Alberi-Morel, "Low-complexity single-image super-resolution based on nonnegative neighbor embedding," 2012.

[46] R. Zeyde, M. Elad, and M. Protter, "On single image scale-up using sparse-representations," in *International conference on curves and surfaces*, 2010.

[47] D. Martin, C. Fowlkes, D. Tal, and J. Malik, "A database of human segmented natural images and its application to evaluating segmentation algorithms and measuring ecological statistics," in *Proceedings Eighth IEEE International Conference on Computer Vision. ICCV 2001*, vol. 2. IEEE, 2001, pp. 416–423.

[48] J.-B. Huang, A. Singh, and N. Ahuja, "Single image super-resolution from transformed self-exemplars," in *Proceedings of the IEEE conference on computer vision and pattern recognition*, 2015, pp. 5197–5206.

[49] Y. Matsui, K. Ito, Y. Aramaki, A. Fujimoto, T. Ogawa, T. Yamasaki, and K. Aizawa, "Sketch-based manga retrieval using manga109 dataset," *Multimedia Tools and Applications*, vol. 76, no. 20, pp. 21 811–21 838, 2017.

[50] C. Dong, C. C. Loy, K. He, and X. Tang, "Image super-resolution using deep convolutional networks," *IEEE transactions on pattern analysis and machine intelligence*, vol. 38, no. 2, pp. 295–307, 2015.

[51] J. Kim, J. Kwon Lee, and K. Mu Lee, "Accurate image super-resolution using very deep convolutional networks," in *Proceedings of the IEEE conference on computer vision and pattern recognition*, 2016, pp. 1646–1654.

[52] K. Zhang, W. Zuo, and L. Zhang, "Learning a single convolutional super-resolution network for multiple degradations," in *Proceedings of the IEEE Conference on Computer Vision and Pattern Recognition*, 2018, pp. 3262–3271.

[53] H. R. Sheikh, Z. Wang, L. Cormack, and A. C. Bovik, "Live image quality assessment database release 2 (2005)," 2005.

[54] A. Foi, V. Katkovnik, and K. Egiazarian, "Pointwise shape-adaptive dct for high-quality denoising and deblocking of grayscale and color images," *TIP*, May 2007.

[55] I. Bello, B. Zoph, A. Vaswani, J. Shlens, and Q. V. Le, "Attention augmented convolutional networks," in *Proceedings of the IEEE/CVF international conference on computer vision*, 2019, pp. 3286–3295.

[56] Z. Zhang, Y. Xu, J. Yang, X. Li, and D. Zhang, "A survey of sparse representation: algorithms and applications," *IEEE access*, vol. 3, pp. 490–530, 2015.

[57] M. Elad and M. Aharon, "Image denoising via sparse and redundant representations over learned dictionaries," *IEEE Transactions on Image processing*, vol. 15, no. 12, pp. 3736–3745, 2006.